Received: 30 June 2023 | Revised: 5 July 2023 | Accepted: 22 August 2023

DOI: 10.1002/pamm.202300151

RESEARCH ARTICLE

Modelling the post-buckling behaviour of steel sheets under induction heating

Vladimir Filkin | **Yury Vetyukov** | **Ben Heinrich** | **Florian Toth**

Institute of Mechanics and Mechatronics, TU Wien, Vienna, Austria

Correspondence
Vladimir Filkin, Institute of Mechanics and Mechatronics, TU Wien, Vienna, Austria.
Email: filkin.vm@gmail.com

Funding information
TU Wien Bibliothek

Abstract

Induction heating has many engineering applications. To accurately describe the induction heating process of thin steel sheets one needs to account for their mechanical deformation. This might strongly affect the magnetic configuration since thin sheets are prone to thermal buckling, leading to large supercritical deformations. We suggest a modelling strategy combining a computationally highly efficient structural mechanical shell description for the thin sheet with a standard continuum model for eddy current and thermal problems through an iterative coupling algorithm. All benchmark problems are solved numerically using the finite element method.

1 | INTRODUCTION

Induction heating is an important technology for many engineering applications. The main reason is that induction heating has several technical advantages over other methods: High power densities allow rapid temperature increase, heat is supplied directly within the target body, no contamination, and others. Designing induction heating systems requires accurate modelling of the magnetic field, the temperature field, and, in many cases, interaction effects: Joule losses from the induced eddy currents are source terms for the thermal problem [1].

Another significant interaction effect is the presence of mechanical deformations caused by thermal expansion. One needs to account for this effect to accurately describe the induction heating of thin steel sheets. Thermal expansion strongly affects the magnetic configuration since thin sheets are prone to thermal buckling, leading to large deformations [2–4]. We suggest a modelling strategy combining a computationally highly efficient mechanical shell description for the thin sheet with a standard continuum model for eddy current and thermal problems through an iterative coupling algorithm. Also, we investigate the post-buckling behaviour of the sheet and its influence on temperature distributions.

2 | GOVERNING EQUATIONS AND NUMERICAL MODELLING

We consider an example of a thin steel sheet moving at a constant velocity. The steel sheet is heated by a single inductor above it, that is, in a single-sided transverse flux heating configuration. The layout of the analyzed structure is presented in Figure 1.

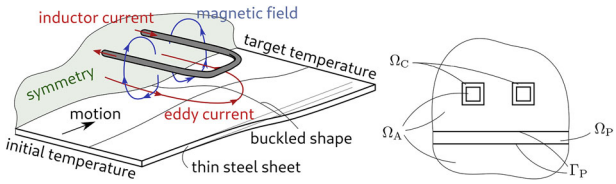

FIGURE 1 Sketch of the analysed system (left) and a cross-section of computational domains (right). An inductor is placed above the moving steel sheet. Eddy currents, induced due to alternating current in the inductor, transfer heat to the sheet. As a result, a steep temperature gradient occurs under the inductor, which leads to thermal buckling of the sheet.

We are interested in the steady-state temperature distribution of the steel sheet. Effects from motion induction and mechanical inertia are neglected, which is appropriate for sufficiently small sheet velocities, present in many technical applications. The action of the harmonically oscillating Lorenz force is neglected, since we are interested in static equilibrium only and not in the vibration behaviour. The static component of the Lorenz force is expected to affect the equilibrium in a similar manner as the assumed initial imperfection. For the sake of simplicity, material properties are assumed to be linear and temperature-independent. The main aim of this contribution is to study the temperature-induced mechanical deformation through buckling, including its feedback onto the magnetic problem.

The governing partial differential equations (PDEs) are solved using the Finite Element Method (FEM). The open-source FE software openCFS [5] is used to solve magnetic and thermal problems. An in-house non-linear shell FEM solver was used for the mechanical part of the model [6].

2.1 | Electromagnetic model

To describe the magnetic field, we consider the eddy-current problem in the frequency domain

$$\nabla \times (\nu \nabla \times \boldsymbol{A}) + \gamma j\omega \boldsymbol{A} = \boldsymbol{J}_i\,, \tag{1}$$

where ν is the magnetic reluctivity and γ the electric conductivity. We solve for the magnetic vector potential $\boldsymbol{A} = \boldsymbol{\nabla} \times \boldsymbol{B}$ defined as the curl of the magnetic flux density. The system is excited by prescribing a total current through the coil. The current density $\boldsymbol{J}_i$ is then resolved from electric ports excitation [7], which allows for the accounting of eddy currents in an inductor region. Thus we arrive at the weak formulation of the problem, including excitation via electric ports,

$$\begin{aligned} \int_{\Omega_{A,P,C}} \nabla \times \hat{\boldsymbol{A}}' \cdot \nu \nabla \times \hat{\boldsymbol{A}} \mathrm{d}\Omega + j\omega \int_{\Omega_{A,P,C}} \gamma \hat{\boldsymbol{A}}' \cdot \hat{\boldsymbol{A}} \mathrm{d}\Omega + \hat{U} \int_{\Omega_C} \gamma \hat{\boldsymbol{A}}' \cdot \nabla V_0 \mathrm{d}\Omega = 0, \\ j\omega \int_{\Omega_C} \gamma \hat{\boldsymbol{A}} \cdot \nabla V_0{}' \mathrm{d}\Omega + \hat{U} \int_{\Omega_C} \gamma \nabla V_0 \cdot \nabla V_0{}' \mathrm{d}\Omega = \hat{I}\,, \end{aligned} \tag{2}$$

where $\hat{U}$ is electric voltage in frequency domain and ∇V_0 denotes a gradient of an electric scalar potential field precalculated at an initial step from the electric flow problem (Poisson) with a prescribed unit voltage difference between ports.

2.2 | Heat conduction model

The temperature field in the steel sheet is modelled by the stationary advection-diffusion equation

$$-\nabla \cdot (\lambda \nabla T - \rho c T \boldsymbol{v}(t)) = \dot{q}\,, \tag{3}$$

where ρ denotes the mass density, c represents the specific heat capacity, λ denotes the coefficient of thermal conduction and $\boldsymbol{v}$ is the velocity of the steel sheet. We solve for the temperature distribution T for known inlet temperature and

heat transfer boundary conditions at the top and bottom of the sheet. The instantaneous volumetric heat source density generated by eddy currents is defined by Joule heating $\dot{q}(t) = \boldsymbol{J}(t) \cdot \boldsymbol{E}(t)$. We use the mean power over one oscillation period given by $\bar{\dot{q}} = \frac{1}{2}\gamma\omega^2|\hat{\boldsymbol{A}}|^2$.

Weak formulation for FEM is

$$\int_{\Omega_P} \nabla T' \cdot (k\nabla T - \boldsymbol{v}\rho c T)\mathrm{d}\Omega + \int_{\Gamma_P} T' h(T - T_r)\mathrm{d}\Gamma = \int_{\Omega_P} T' \bar{\dot{q}}\mathrm{d}\Omega\,, \tag{4}$$

where h is a heat transfer coefficient and T_r denotes a reference temperature of the surrounding media.

2.3 | Mechanical shell model

Thermal expansion due to the inhomogeneous temperature field leads to deformations of the steel sheet. The mechanical equilibrium configuration is obtained by assuming linear, isotropic thermal expansion for an isotropic and linear elastic material. Geometric nonlinearities must be accounted for to be able to describe the post-buckling behaviour of the structure. In order to obtain a computationally efficient solution, we represent the thin steel sheet as a material surface, that is, by using a Kirchhoff-Love shell model [6]. Weak formulation for the problem of static equilibrium of the shell follows from the principle of minimality of the total potential energy of a mechanical system

$$U^{\text{total}} = U^{\text{strain}} + U^{\text{ext}} \to \min, \quad U^{\text{strain}} = \int_{\Omega_{\text{shell}}} U(\boldsymbol{E}, \boldsymbol{K})\mathrm{d}\Omega\,, \tag{5}$$

where U^{ext} denotes the potential of the external forces, U is the elastic strain energy density and $\boldsymbol{E}$ and $\boldsymbol{K}$ are strain tensors. Strain energy density has a quadratic form

$$\begin{aligned} &U(\boldsymbol{E}, \boldsymbol{K}) = \frac{1}{2}(E_1(\mathrm{tr}\boldsymbol{E})^2 + E_2\boldsymbol{E}\cdot\cdot\boldsymbol{E} + D_1(\mathrm{tr}\boldsymbol{K})^2 + D_2\boldsymbol{K}\cdot\cdot\boldsymbol{K}),\\ &\boldsymbol{E} = \frac{1}{2}(\boldsymbol{F}^{\mathrm{T}}\cdot\boldsymbol{F} - \mathring{\boldsymbol{a}}(T)), \quad \boldsymbol{K} = \boldsymbol{F}^{\mathrm{T}}\cdot\boldsymbol{b}\cdot\boldsymbol{F} - \mathring{\boldsymbol{b}}, \quad \mathring{\boldsymbol{a}}(T) = (1+\alpha T)(\boldsymbol{I} - \boldsymbol{nn}), \quad \mathring{\boldsymbol{b}} = -\nabla\boldsymbol{n}, \end{aligned} \tag{6}$$

where $\boldsymbol{a}$, $\boldsymbol{b}$, $\mathring{\boldsymbol{a}}(T)$ and $\mathring{\boldsymbol{b}}$ are the first and the second metric tensors in current and reference configurations respectively, $\boldsymbol{n}$ is the unit normal vector in the reference configurations, $\boldsymbol{F}$ is a deformation gradient, and α is a thermal expansion coefficient. Thermal expansion is included in the first metric tensor of the reference configuration.

2.4 | Coupling

Since the mechanical shell model of the steel sheet is based on the deformation of a reference surface only, we need to update the three-dimensional geometry used in the magnetic and thermal problems consistently. Likewise, the through-the-thickness temperature distribution obtained in the three-dimensional thermal model must be used to compute the thermal strain and curvature of the reference surface. For both steps, an interpolation of the finite element results from one grid to the other grid is required. Since the sheet geometry is simple, we use a structured mesh which makes the interpolation more straightforward than for general meshes.

In order to account for the interaction between mechanical deformation and magnetic fields, we use an iterative procedure: First, we compute the magnetic field and resulting eddy currents for a given impressed current density in the inductor. The period averaged eddy current (Joule) losses are then applied as heat source density to the thermal problem. The solution of the advection-diffusion equation is the temperature field in the steel sheet. Next, the temperature distribution is transferred to thermal strains and curvature changes as a thermal load for the shell model, which is needed at the integration points of the shell elements. After the solution of the non-linear mechanical problem, the deformed equilibrium configuration of the reference surface is transferred to the 3D magnetic and thermal problem as a mesh update Figure 2. The magnetic problem is then re-computed for the updated grid continuing the iteration. The

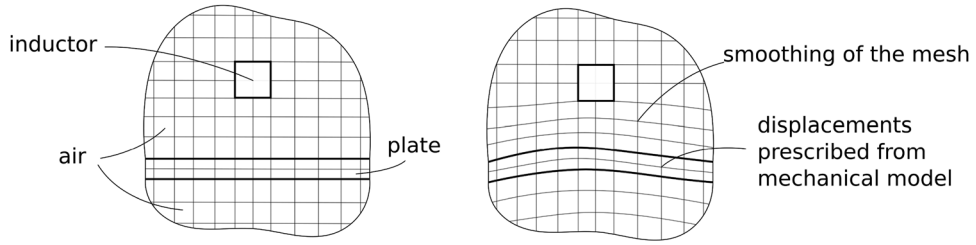

FIGURE 2 The grid smoothing procedure: the initial grid (left) and the grid after "smoothing" (right). Displacements from a solution of the shell model are applied as BCs to the sheet domain and then smoothed in the air domain.

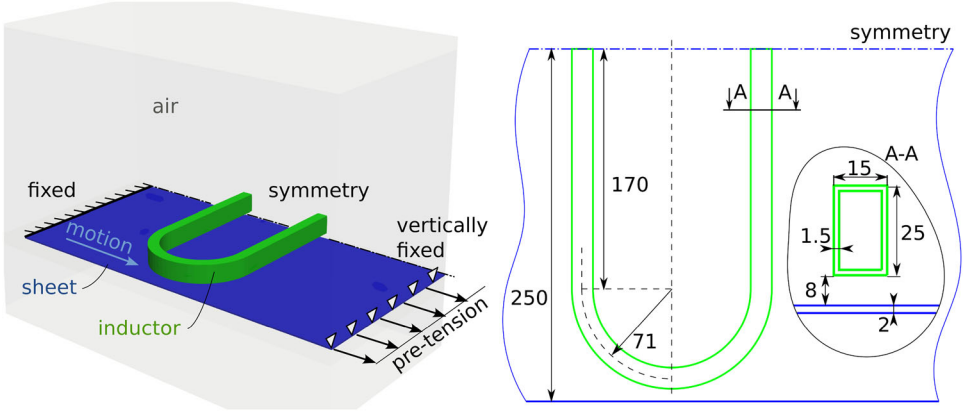

FIGURE 3 The studied model. BCs and loads on the left and dimensions on the right (in mm). Due to symmetry, only half of the model is investigated. We prescribe the total current in the inductor. The inlet temperature is zero, and heat transport boundary conditions are applied on the top and bottom sides of the sheet. The sheet is fixed in normal and length directions at the inlet, and pre-tension is applied at the outlet.

iteration is terminated once a suitable convergence criterion, for example, based on the relative change of the field quantities between iterations.

The update of the grid is achieved by solving the grid smoothing equation

$$\frac{1}{2}\int_{\Omega_{\mathrm{P,A}}} \mathbf{B}(\mathbf{u}') : \mathbf{C} : \mathbf{B}(\mathbf{u})\mathrm{d}\Omega = 0, \quad \mathbf{B}(\mathbf{u}) = \frac{1}{2}(\nabla\mathbf{u} + (\nabla\mathbf{u})^{\mathrm{T}}) \tag{7}$$

which resembles standard linear small-strains mechanical equation without any force terms. As BCs, we apply displacements from shell modelling results on the upper and lower surfaces of the sheet.

3 | APPLICATION EXAMPLE

3.1 | Model

The computational procedure is tested on a simple but application-oriented test case Figure 3: The steel sheet is 2 mm thick and 0.5 m wide and moves with a speed of 0.1 m s^{-1}. The length of the sheet is 0.5 m for the electromagnetic and heat conduction models and 1 m for the mechanical model. The material parameters are presented in Table 1.

For the electromagnetic model, we applied flux parallel boundary conditions for the outer surfaces of our model. We studied the range of applied current amplitudes corresponding to the pre-buckling, buckling, and post-buckling behaviour. The field solutions were investigated with 4400 A current amplitude. For the load-displacement curve we investigated total currents of 2400, 3600, 3800, 3900, 4000, 4200, 4400, 4600 and 4800 A. The frequency is 5400 Hz for all the EM computations. Regarding the heat conduction model, at the inlet of the sheet, we applied homogeneous Dirichlet BC. At the top and the bottom of the sheet, we assumed heat transport BC with zero bulk temperature and heat transfer coefficient

TABLE 1 Material properties.

Material parameter	Sheet	Inductor	Air
Magnetic permeability in H m^{-1}	1.26×10^{-5}	1.26×10^{-6}	1.26×10^{-6}
Electric conductivity in S m^{-1}	1.00×10^{6}	5.96×10^{7}	
Heat capacity in J K^{-1} kg^{-1}	420		
Heat conductivity in W m^{-1} K^{-1}	45		
Thermal expansion coefficient in K^{-1}	12.0×10^{-6}		
Density in kg m^{-3}	7800		
Young's modulus in GPa	100		
Poisson's ratio	0.3		

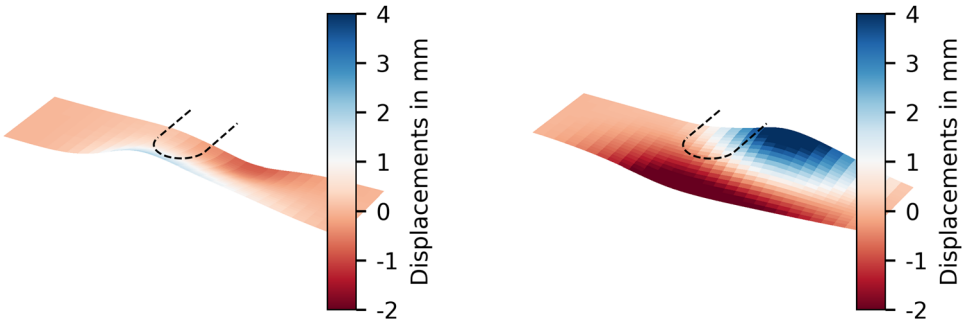

FIGURE 4 Deformed shapes of the steel sheet for different initial imperfections under the same current loading. Direct - on the left, and reverse - on the right. The amplitude of deflections for the direct case is lower than for the reverse one.

equal to 20 W m^{-2} K^{-1}. For other surfaces, homogeneous Neuman BCs were chosen. As mechanical BCs and loading, we fixed the inlet of the sheet, fixed normal displacements, and applied pre-tension 20 000 N m^{-1} on the outlet.

3.2 | Field results

The deformation figure represents a typical buckled shape, indicated by the severe out-of-plane deflections (the trivial equilibrium only contains in-plane deformations). Under defined conditions, the sheet experiences two forms of buckling based on initial imperfection (curvatures of the sheet with different signs) Figure 4. We call them direct (the middle of the sheet buckles away from the inductor) and reverse (the middle buckles towards). In the case of pure thermal buckling, when the heat source doesn't depend on the post-buckling behaviour, these forms differ only by the direction of deflections.

The temperature distributions for non-deformed, direct, and reverse cases are depicted in Figure 5. The right graph represents the temperature over the width of the sheet at the very right side of it (outlet). Deflections towards the coil cause a local temperature increase, and the opposite effect is observable for the deflections away from the coil. For the direct configuration, one can see a significant temperature increase under the u-turn of the coil. For the reverse configuration, an increase is located right at the symmetry plane. The temperature differences in different configurations are related to the changes in eddy current distribution from an electromagnetic model. Redistribution of the eddy currents inside the sheet due to deflections changes the Joule loss density, thus changing the temperature field.

3.3 | Load-displacement curve

In Figure 6, load-displacement curves for different points of the sheet are presented. The load is a total input current in the inductor. In the figure, we have two branches of the graph with different signs of deflections. Two branches of the curves resemble two branches of ordinary post-buckling behaviour of a beam [8]. The main difference is non-symmetry of the branches caused by the influence of the inductor placed only from one side of the sheet. Another difference one

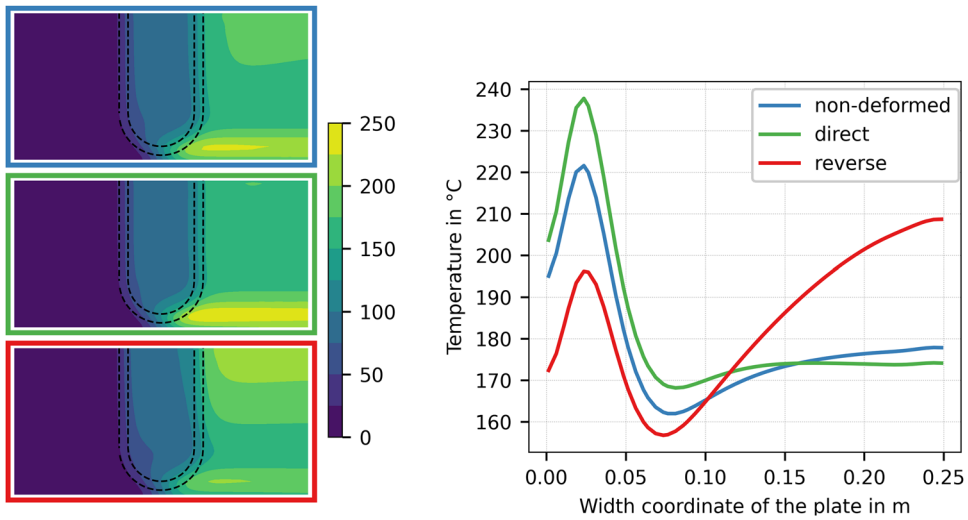

FIGURE 5 The temperature field (in °C) in the steel sheet. On the left: the colour plot over the upper surface of the sheet for (from top to bottom) non-deformed, direct, and reverse configurations. On the right: the graph representing the temperature over the width of the sheet at the very right side.

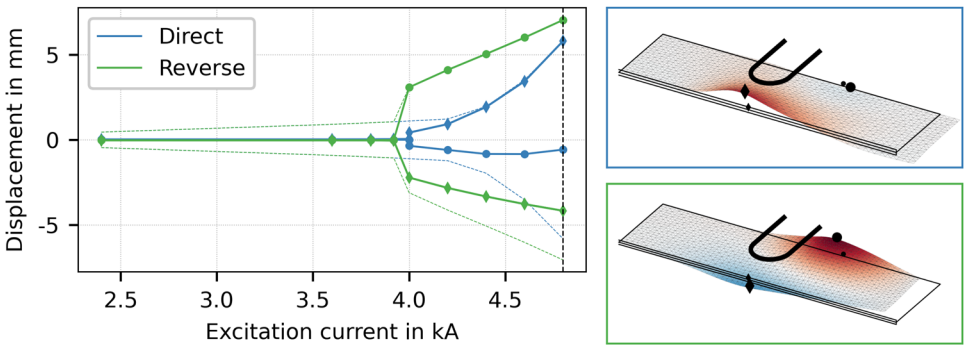

FIGURE 6 Load-displacement curve for two different points on the sheet (marked by rhombuses and circles) and two different configurations: direct and reverse (left). The buckled shapes corresponding to the peak load: direct configuration (right-top) and reverse configuration (right-bottom).

can notice is a rapid jump of the deflections for the reverse and direct graphs. We assume that it is an instability region in post-buckling behaviour. This means that having a load infinitely small above critical, we get a significant increase in deflections of the sheet.

The other significant difference is the buckling shape, which makes load-displacement curves at different points of the sheet behave differently. One can see it from the comparison of curves representing different points of the sheet (with circular and rhombus markers) in Figure 6.

4 | DISCUSSION

Buckling occurs with the current amplitudes introducing the sharp temperature rise by 200 K: Load-displacement curve demonstrates non-symmetrical behaviour and the unstable rapid change of deflections. Both phenomena significantly affect the results of the computations and should be accounted in a designing process.

Since the distance of the steel sheet to the inductor is an important parameter in the magnetic system, the buckling deformation is expected to have a significant impact. Taking the deformation into account in the magnetic model allows for an accurate description of the problem. This is the first step in exploiting the often unavoidable bucking positively, for example, by accounting for the predicted steel sheet shape when optimizing the inductor geometry. Using a

structural mechanical shell element model to compute the post-buckling deformation is computationally highly efficient. The approach can be extended to other configurations involving thin-walled structures.

ACKNOWLEDGMENTS

The authors acknowledge TU Wien Bibliothek for financial support through its Open Access Funding Programme.

ORCID

Vladimir Filkin https://orcid.org/0000-0001-5925-8418
Florian Toth https://orcid.org/0000-0002-4632-4436

REFERENCES

1. Roppert, K., Toth, F., & Kaltenbacher, M. (2019). Simulating induction heating processes using harmonic balance FEM. *COMPEL - The International Journal for Computation and Mathematics in Electrical and Electronic Engineering*, *38*(5), 1562–1574.
2. Zhu, Y., & Luo, Y. (2018). Fully coupled magneto-thermo-structural analysis by morphing method and its application to induction heating process for plate bending. *International Journal of Applied Electromagnetics and Mechanics*, *56*, 573–583.
3. Kadkhodaei, G., Sheshyekani, K., & Hamzeh, M. (2016). Coupled electric-magnetic-thermal-mechanical modelling of busbars under short-circuit conditions. *IET Generation, Transmission and Distribution*, *10*, 955–963.
4. Takagaki, M., & Toi, Y. (2009). Coupled analysis of induction hardening considering induction heating, thermal elasto-viscoplastic damage, and phase transformation. *International Journal of Damage Mechanics*, *19*, 321–338.
5. openCFS v2022W (2022). https://opencfs.org/.
6. Vetyukov, Y. (2014). Finite element modeling of Kirchhoff-Love shells as smooth material surfaces. *ZAMM - Journal of Applied Mathematics and Mechanics / Zeitschrift für Angewandte Mathematik und Mechanik*, *94*.
7. Roppert, K., Toth, F., & Kaltenbacher, M. (2020). Modeling nonlinear steady-state induction heating processes. *IEEE Transactions on Magnetics*, *56*(3), 1–4.
8. Eslami, M. R. (2018). *Buckling and post-buckling of beams* (pp. 7–110). Springer International Publishing.

How to cite this article: Filkin, V., Vetyukov, Y., Heinrich, B., & Toth, F. (2023). Modelling the post-buckling behaviour of steel sheets under induction heating. *Proceedings in Applied Mathematics and Mechanics*, *23,* e202300151. https://doi.org/10.1002/pamm.202300151